Lithosphere

Research Article

Experimental Research on the Effect of Bedding Angle on the Static and Dynamic Behaviors of Burst-Prone Sandstone

Peng Tang [iD],[1] Xiang Ma,[2] Yang Zhao [iD],[1] Lishuai Jiang [iD],[1,3] Kegong Fan,[1] Xiaoyu Hu,[1] and Fangtian Wang[4]

[1]State Key Laboratory of Mining Disaster Prevention and Control, Shandong University of Science and Technology, Qingdao 266590, China
[2]Inner Mongolia Zhongtai Energy Co., Ltd., Yiqi Branch, Ordos 017000, China
[3]State Key Laboratory of Mining Response and Disaster Prevention and Control in Deep Coal Mines, Anhui University of Science and Technology, Huainan 232001, China
[4]School of Mines, China University of Mining and Technology, Xuzhou 221116, China

Correspondence should be addressed to Yang Zhao; mrzhao_y@163.com and Lishuai Jiang; lsjiang@sdust.edu.cn

In order to understand the mechanism of some unconventional failures such as rockburst caused by deep rock excavation, the failure characteristics of burst-prone sandstone specimens under static and dynamic loads were studied by using the MTS816 rock mechanics testing system and the split Hopkinson pressure bar (SHPB) experimental system, as well as the effects of bedding angle and impact pressure on rock mechanical properties and failure patterns. The uniaxial compression test used a cylindrical specimen with a height of 50 mm and a diameter of 100 mm, and cylindrical specimens with height and diameter of 50 mm were adopted in the SHPB tests. The bedding angles in the tests are 0°, 45°, and 90°. In the dynamic impact test, three different impact pressures were applied to observe the magnitude of impact load on the mechanical behaviors of the burst-prone sandstone specimens. The results show that with the increase in the bedding angle, the uniaxial compressive strength firstly decreases and then increases. When the bedding angle is 45°, the uniaxial compressive strength is the lowest. The uniaxial compressive strength is highest when the bedding angle is 0°. The burst-prone sandstone specimens with different bedding angles had three different failure pattern types. Under the dynamic loading, the stress-strain curves show springback phenomenon; with the increase in impact pressure, the dynamic strength of the burst-prone sandstone specimens with each bedding angle increases; the fracture degree of the bedding sandstone specimens gradually increases. The dynamic strength of the 45° burst-prone sandstone specimen is the lowest, and it has the highest fracture degree.

1. Introduction

As a complex geological body, under the influence of various factors such as long-term geological action and different occurrence conditions, rock mass has structural surfaces such as bedding structures, fissures, and faults [1, 2]. The mechanical properties of rock mass caused by these structural surfaces are quite different from intact rocks. Sandstone is a common rock mass in engineering. Under the action of geological structure, it has obvious characteristics of bedding structure and significant anisotropism. The degree of particle cementation along the bedding direction is relatively weak, and the bedding plane is weak relative to the rock matrix. The failure characteristics and mechanical properties of bedding rock mass show obvious anisotropism after loading [3, 4]. There are also multiple combinations of the direction of the bedding plane and the direction of the main load. The corresponding mechanical properties and deformation characteristics have an important impact on the safety and stability of rock mass engineering. Therefore, understanding the effect of bedding angle on rock dynamic and static mechanical properties and failure patterns is of great significance to the stability and safety assessment of rock engineering.

At present, regarding the mechanical properties of bedding rocks, many scholars have explored a lot of research and achieved fruitful results. With respect to static mechanical properties of bedding rocks, Tien and Kuo [5] put forward the failure criterion of anisotropic rocks based on two different failure patterns of specimens by performing uniaxial compression tests on specimens with different beddings. Wang et al. [6] carried out uniaxial compression tests with bedded slate and found that bedding planes with different dip angles are the main reasons for the different fracture modes of slate. Tavallali and Vervoort [7] conducted a Brazilian splitting test for sandstone materials, and the relationship between tensile strength and failure cracks and the variation of bedding angle was investigated. Yang et al. [8] studied the difference in mechanical properties between horizontally and vertically bedded rock samples through conventional triaxial tests and Brazilian splitting tests. Zhou et al. [9] performed a Brazilian splitting test on layered rocks and proposed an enhanced equivalent continuous model of layered rocks and verified it by numerical simulations. However, in many mining engineering applications, such as rock cutting, drilling, tunneling, rock blasting, and rock bursting, rock mass is stressed dynamically [10]. With respect to dynamic mechanical properties of bedding rocks, Zhang et al. [11] used five groups of different dip angle samples to study the effect of layers on the dynamic compressive behaviors and failure patterns of transversely isotropic rocks. Qiu et al. [12] studied the phyllite with different dip angles by dynamic Brazilian tensile tests and discussed the associated fracturing development. Liu et al. [13] conducted quasi-static and dynamic uniaxial compression tests on coal rock and found that the dynamic strength exhibits distinct variations in different bedding directions.

In summary, although some scholars have carried out related research on the static and dynamic mechanical properties of bedding rock masses, there are few studies on the dynamic mechanical properties of bedding rock masses under different bedding angles and impact pressures. The key influencing factors of dynamic failure of rock mass are still not clear, for example, what is the influence of the magnitude of dynamic load on failure patterns of bedding rock mass. Therefore, this paper uses the MTS816 rock mechanics test system and the split Hopkinson pressure bar (SHPB) experimental system to carry out the uniaxial compression test and the dynamic impact test of the burst-prone sandstone specimens with different bedding angles. The mechanical properties and failure patterns under static load and impact load state are studied, with the help of the SHPB test device to provide different dynamic impact pressure loads, and the failure patterns of sandstone specimens with different bedding angles are discussed.

2. Mechanical Behaviors and Failure Patterns of Bedding Sandstone under Uniaxial Compression

2.1. Uniaxial Compression Test Method for Bedding Sandstone.
The rocks used for the experiment are collected from the

FIGURE 1: Sandstone specimens with different bedding angles.

Hongqinghe coal mine, located in the Inner Mongolia, China. The 3-1 coal seam is the main mining and first mining coal seam. The average thickness of the coal seam is 6.98 m, the average burial depth is 755 m, the geological conditions of the coal seam are simple, and the occurrence of coal seam is stable. Above the roof are mainly siltstone, medium/fine-grained sandstone, and medium conglomerate, and there is no weak sandstone between each rock layer, forming a composite thick rock layer. The floor is mainly sandy mudstone, sandstone, and siltstone, mainly semihard rock. Affected by the large mining height, large burial depth, and the mining, during the mining of the panel 3101, the head entry (1) of panel 3103 had serious roof fall, floor heave, and rib fall. The lithology is burst-prone sandstone, and the bedding structure is significant. Therefore, in order to understand the mechanical behaviors of surrounding rock near the rockburst accident area, the floor rock mass near the panel 3103 were sampled. The large sandstones with bedding taken from the coal mine are brought back to the laboratory, the specimens are drilled and ground, and then after the cutting and polishing process [14], a standard cylindrical specimen with a diameter of 50 mm and a height of 100 mm following the method suggested by the International Society for Rock Mechanics (ISRM) [15] is obtained, as shown in Figure 1. The ends of the specimens are ground and polished to unevenness and nonperpendicularity to less than 0.02 mm, and all test specimens are stored in a dry environment at room temperature. Furthermore, it should be noted that α represents the bedding angle. In this study, three bedding angles (0°, 45°, and 90°) are considered.

The uniaxial compression test uses the MTS816 rock mechanics test system, as shown in Figure 2. It can record and store the parameters such as stress, strain, and time of the specimen in real time. The uniaxial compression loading control adopts the displacement loading method, and the load is applied to the sandstone specimen with the axial loading rate of 0.5 mm/min.

2.2. Influence of Bedding Angles on the Static Mechanical Behaviors of Burst-Prone Sandstone.
Typical stress-strain curves for the sandstone specimens with different bedding
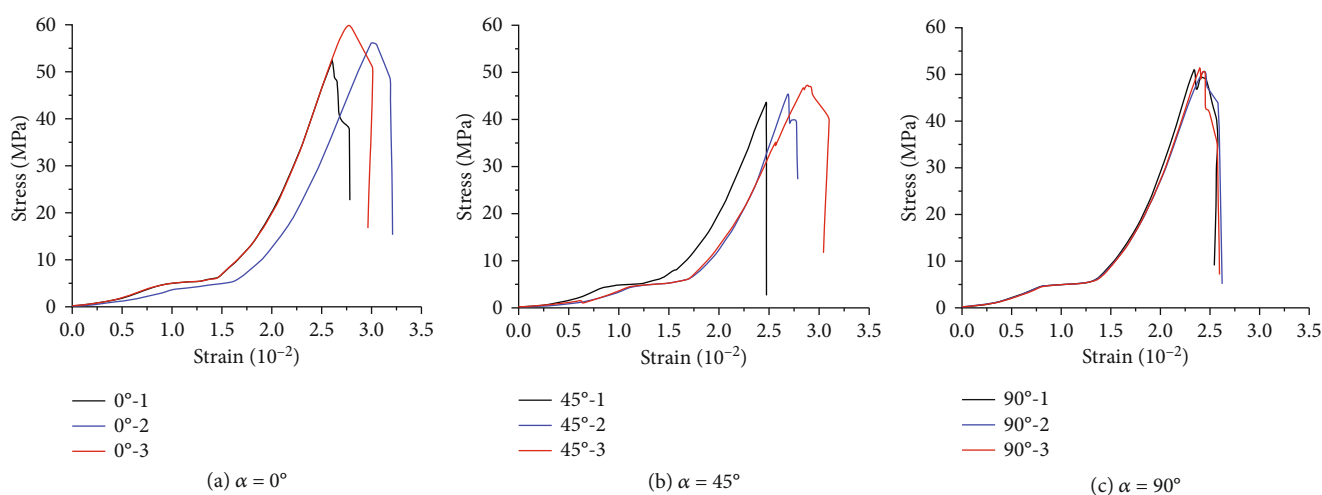
Figure 2: MTS816 rock mechanics test system.

(a) $\alpha = 0°$

(b) $\alpha = 45°$

(c) $\alpha = 90°$

Figure 3: Stress-stain curves of bedding sandstone specimens under uniaxial compression.

angles under the uniaxial compression test are presented in Figure 3, which indicates that bedding angles have a significant influence on the mechanical behaviors of sandstone.

As shown in Figure 4, the stress-strain curves of the bedding sandstone specimens closest to the average value of peak strength were selected for comparison.

The specific test results of the uniaxial compression testing are listed in Table 1. Figure 5 shows the variation law of peak strength and modulus of elasticity of sandstone specimens with different bedding angles. According to the stage characteristics of bedding sandstone deformation evolution, the stress-strain curves of all bedding sandstone specimens can be approximately divided into four stages: (1) pore compaction stage, (2) linear elastic deformation stage, (3) elastoplastic deformation stage, and (4) postpeak stage. When the stress increases to the peak strength, the bedding sandstone specimens suddenly fail, and the mechanical behavior of the sandstone specimens with all bedding angles shows the characteristics of brittle fall [16]. With the increase in the bedding angle, the uniaxial compressive strength of the specimens shows a change rule of first decreasing and then increasing. When $\alpha = 0°$, the peak strength of the sandstone
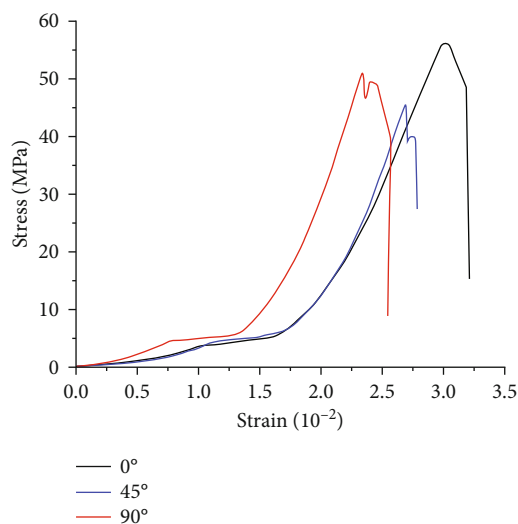

Figure 4: Comparison of specimens with different bedding angles.

TABLE 1: Mechanical parameters of the specimen.

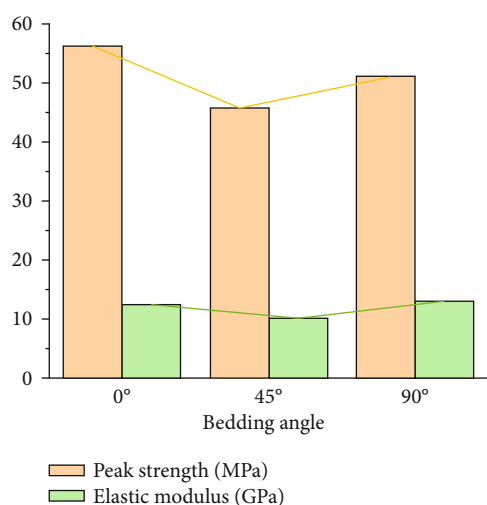| Specimen number	Bedding angle	Modulus of elasticity (GPa)	Average modulus of elasticity (GPa)	Peak strength (MPa)	Average peak strength (MPa)
0°-1		12.29		52.44	
0°-2	0°	11.58	12.47	56.30	56.26
0°-3		13.54		60.03	
45°-1		10.14		44.01	
45°-2	45°	9.99	10.14	45.71	45.74
45°-3		10.30		47.51	
90°-1		13.21		51.12	
90°-2	90°	12.91	13.08	50.78	51.14
90°-3		13.11		51.53	

FIGURE 5: The strength parameters of bedding sandstone specimens.

specimen is the highest, and the average value is 56.26 MPa; the peak strength of the sandstone specimen with a bedding angle of 45° is the lowest, with an average value of 45.74 MPa, a decrease of 18.7%.

With the increase in the bedding angle, the modulus of elasticity of the sandstone specimen first decreased and then increased, which was basically consistent with the variation law of the uniaxial compressive strength of the sandstone. When $\alpha = 45°$, the modulus of elasticity is the smallest, with an average value of 10.14 GPa, followed by 0°, and the largest value is at $\alpha = 90°$, with an average value of 13.08 GPa. In conclusion, the bedding angle has a significant effect on the static mechanical properties of burst-prone sandstone specimens.

2.3. Failure Behavior of Bedding Sandstone under Uniaxial Compression. The bedding angle not only has a significant effect on the peak strength of the sandstone specimen but also has a certain effect on the failure patterns of the sandstone specimen [17, 18]. Figure 6 depicts the uniaxial failure

patterns of the sandstone specimen with different bedding angles. Under the action of uniaxial compression, when $\alpha = 0°$, the macroscopic cracks in the sandstone specimen are mainly vertical cracks running through the bedding, the failure pattern is mainly longitudinal column splitting failure, and there is local compression and expansion phenomenon in the sandstone specimen. During axial compression, the axial deformation of the sandstone specimen is suppressed, and the specimen will expand in the radial direction. Under the action of tensile stress, the cracks parallel to the axis of the specimen appear, and they merge and penetrate each other; eventually, the sandstone specimen loses its ability to resist external loads.

When $\alpha = 45°$, due to the obvious weak structural plane, the sandstone specimen has low shear strength and stress concentration is more likely to occur on the bedding plane. When the specimen is loaded in the axial direction, the shear stress of the bedding plane exceeds its shear strength value. Later, the sandstone specimen will slip and fail along the direction of the bedding plane, forming macroscopic cracks, mainly shear failure as a whole, and local tensile cracks occur. The fracture surface is roughly along the 45° direction. The uniaxial compressive strength of this sandstone specimen is mainly determined by the bond strength of the weak plane of the bedding [19], which is consistent with the aforementioned uniaxial compressive strength analysis results.

When $\alpha = 90°$, the sandstone specimen is roughly conical after failure, and the circle around the specimen is the first to fall off, and the degree of fragmentation is relatively large. It can be seen that the failure pattern is tension and shear failure. After analysis, it is found that the formation of this failure pattern is caused by the large friction between the upper and lower ends of the sandstone specimen and the bearing plate of the testing machine. The friction force between the end face of the specimen and the bearing plate makes the end face of the specimen form a hoop function, and this action weakens as it moves away from the bearing plate, making it appear as a tensile stress. In the tensile stress area, due to the lateral deformation and peeling freely, a conical failure pattern is finally formed.

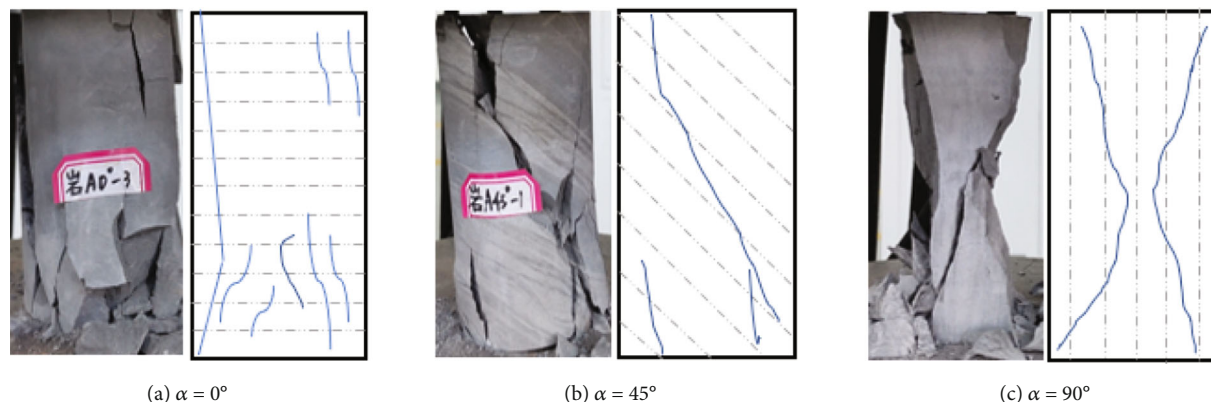(a) $\alpha = 0°$ (b) $\alpha = 45°$ (c) $\alpha = 90°$

FIGURE 6: Failure patterns of bedding sandstone specimens under uniaxial compression.

It can be seen from the above analysis that under uniaxial compression, with the increase in the bedding angle, the failure pattern of the bedding sandstone specimen changes from splitting and tension failure running through the bedding to a shear slip failure along the bedding plane and then transforms into a conical failure form. The distribution of bedding angle is the main factor leading to the difference in failure patterns of sandstone specimens, and the different failure patterns also determine the anisotropic distribution characteristics of the compressive strength and deformation modulus of bedding sandstone specimens [20].

2.4. Summary of the Effect of Bedding Angle on the Static Mechanical Properties of Burst-Prone Sandstone. The burst-prone sandstone used in the uniaxial compression test was taken from the Hongqinghe coal mine, with a significant bedding weak plane, and uniaxial compression tests were conducted on sandstone specimens with different bedding angles using the MTS816 rock mechanics test system; it is found that the morphology of stress-strain curves during the loading process of burst-prone sandstone specimens with different bedding angles is basically the same, and they all go through the pore compaction stage, linear elastic deformation stage, elastoplastic deformation stage, and postpeak stage. With the increase in the bedding angle, the pore compaction stage of the stress-strain curve gradually becomes shorter, the stress-strain curve gradually becomes steeper, and the peak stress of the burst-prone sandstone specimens shows a trend of first decreasing and then increasing; it is lowest when $\alpha = 45°$.

The failure pattern of the burst-prone sandstone specimen is closely related to the bedding angle, and it can be generally summarized into three types: splitting and tension failure running through the bedding, shear slip failure along the bedding plane, and conical failure form.

The bedding plane is the weak link of bedding rock mass, which is the root cause of the difference in strength and deformation failure characteristics of bedding rock mass. In the analysis of underground mining, engineering slope, tunnel design, and deformation stability related to bedding rock mass, the influence of bedding angle on

FIGURE 7: Cylindrical specimen for SHPB tests.

the mechanical properties and failure pattern of rock mass cannot be ignored.

3. Dynamic Behaviors and Failure Patterns of Bedding Sandstone under Dynamic Load

3.1. Dynamic Impact Test Method of Bedding Sandstone. To clarify the dynamic mechanical properties of bedding sandstone under dynamic loading and realize the research on the failure mechanism of bedding sandstone under different dynamic disturbances, sandstone specimens with different bedding angles were used to carry out dynamic impact tests using the SHPB test system. According to the test requirements [21], the sandstone specimen is a cylindrical specimen with a diameter of 50 mm and a length-to-diameter ratio of 1 : 1, as shown in Figure 7. The sampling location and processing procedures are the same as those specimens used for the uniaxial compression test.

The laboratory tests used the combined dynamic and static loading SHPB device of Hunan University of Science and Technology with a 50 mm bar diameter and medium and high strain rate. The semisine stress loading wave generated by the special-shaped punch can achieve constant strain rate loading. At the same time, the SHPB system is equipped with a superdynamic strain gauge, oscilloscope, and data processing device, which can realize the functions of stress wave signal acquisition and recording and data processing. The system composition is shown in Figure 8. Based on
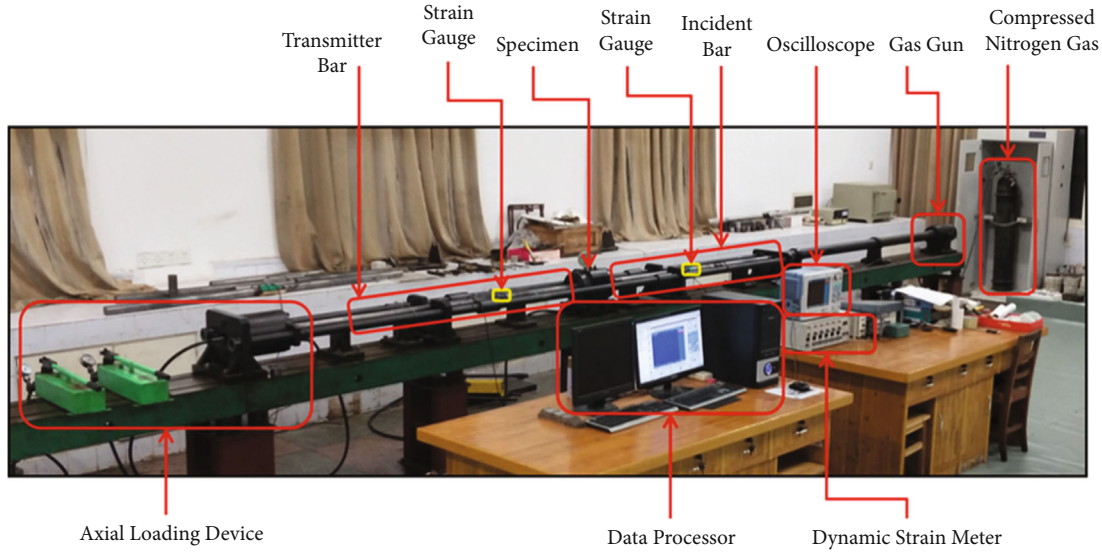
FIGURE 8: Schematic diagram of the SHPB experimental test system.

the one-dimensional stress wave theory [22], the mechanical parameters such as the dynamic stress $\sigma(t)$, strain $\varepsilon(t)$, and strain rate $\dot{\varepsilon}(t)$ of the specimen can be obtained by the following formula [23]:

$$
\begin{aligned}
\sigma(t) &= \frac{A_e}{2A_s}[\sigma_I(t) - \sigma_R(t) + \sigma_T(t)], \\
\varepsilon(t) &= \frac{1}{\rho_e C_e L_s} \int_0^t [\sigma_I(t) + \sigma_R(t) - \sigma_T(t)]dt, \qquad (1)\\
\dot{\varepsilon}(t) &= \frac{1}{\rho_e C_e L_s}[\sigma_I(t) + \sigma_R(t) - \sigma_T(t)],
\end{aligned}
$$

where A_e, ρ_e, and C_e are the cross-sectional area, density, and P-wave velocity of the elastic bar, respectively. A_s and L_s are the cross-sectional area and length of the specimen, respectively. $\sigma_I(t)$, $\sigma_R(t)$, $\sigma_T(t)$ are the incident stress, reflected stress, and transmitted stress of the bar at time "t," respectively.

To minimize the influence of specimen heterogeneity on the test results, the basic parameters such as quality and density of each sandstone specimen are measured before the tests, and then, sandstone specimens with similar physical parameters were selected for dynamic impact tests. The sandstone specimens are divided into three groups ($\alpha = 0°$, 45°, and 90°) according to the different bedding angles for dynamic impact tests. During the test, the impact pressure is controlled by the regulating steam valve on the compressed nitrogen gas. Before setting the impact pressure level, the specimens were pretested under different impact pressure loading, and when the specimens started to have obvious macroscopic damage, the impact pressure at this time was determined to be the minimum impact pressure level, and after determining the minimum impact pressure level to be 0.45 MPa, the subsequent impact pressure gradient was set with an impact pressure difference of 0.05 MPa. And from the perspective of strain rate, the three impact

pressure levels set for the test can meet the required strain rate for the test. Therefore, the existing three impact pressure levels were set by combining the above factors. After pretesting, the impact pressure is set to three levels: 0.45 MPa, 0.50 MPa, and 0.55 MPa, represented by D_1, D_2, and D_3, respectively. The specific SHPB test plan is shown in Table 2.

To reduce the lateral friction between the specimen and the bar, a layer of lubricant was evenly applied to both ends of the specimen when placing the specimen, and good contact between the specimen and the elastic rod was ensured. During the SHPB test, the spindle-shaped punch is fixed in the same position of the launch chamber in each test, and the dynamic load of the predetermined impact pressure is applied through the compressed nitrogen gas to make the test reach the required loading conditions. The schematic diagram of the loading state of the specimen is shown in Figure 9.

To ensure the correctness of the SHPB test results, under the action of dynamic load, both ends of the sandstone specimen must reach dynamic stress balance before the sandstone specimen fails [24, 25]. The dynamic stress wave curves at both ends of the specimen are shown in Figure 10. It can be seen that the transmitted stress wave $\sigma_T(t)$ basically coincides with the superimposed wave of the incident stress wave $\sigma_I(t)$ and the reflected stress wave $\sigma_R(t)$, indicating that the specimen can achieve and maintain the dynamic stress equilibrium condition during the dynamic loading process; thus, the validity of the SHPB test results is verified.

3.2. Dynamic Stress-Strain Curves of Bedding Sandstone Specimens. Under different impact pressures, the dynamic stress-strain curves obtained by the dynamic impact test on sandstone specimens with different bedding angles are plotted in Figure 11. The sandstone specimens were damaged under various loading conditions. The dynamic impact test results are shown in Table 3. The dynamic strength in

TABLE 2: Dynamic load test scheme.

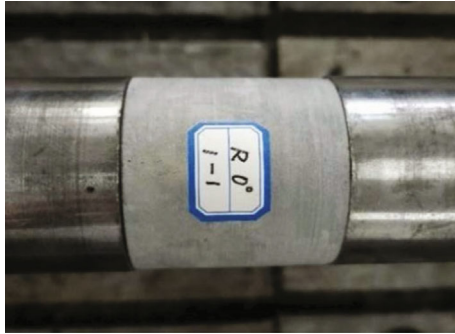| Specimen number			Impact pressure (MPa)
0°-D_1	45°-D_1	90°-D_1	0.45
0°-D_2	45°-D_2	90°-D_2	0.50
0°-D_3	45°-D_3	90°-D_3	0.55

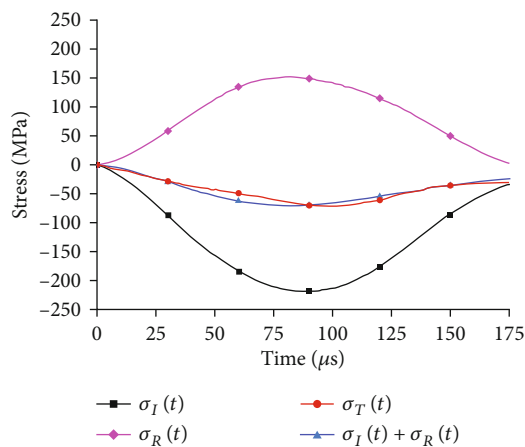FIGURE 9: Impact loading state of the sandstone specimen.

FIGURE 10: Stress equilibrium curves of the specimen.

Table 3 is the peak stress of the dynamic stress-strain curve, which reflects the impact resistance of the sandstone specimen.

It can be seen from Figure 11 that the dynamic stress-strain curve of the bedding sandstone specimen can be roughly divided into five stages. Taking the dynamic stress-strain curve of specimen 0°-D_1 as an example, the first stage curve OA is different from the initial stage of the general static load curve; it does not show an upward concave shape but is closer to a form of approximate elastic change; the modulus is large at this time, indicating that under the action of impact load, the impact rod loading speed is fast, and the closing and compaction time of microcracks in the sandstone is short in a short time, so the compaction stage of pores and cracks is not obvious, showing high impact toughness and strength. The dynamic stress-strain relationship in the second stage AB is a nonlinear relationship. In this stage, the stress-strain slope gradually decreases, the

compressive modulus starts slowly relative to the initial modulus, and the stress rises slowly. This stage shows that the microcracks in the sandstone begin to increase under the action of dynamic load, resulting in a decrease in modulus. In the third stage BC, the compressive modulus decreased significantly, indicating that the microcracks in the sandstone began to expand rapidly under the action of the stress wave [26]. When reaching the peak strength, the specimen macroscopically failed; in the fourth stage CD, after the strength of the sandstone specimen reached the peak strength, the stress gradually decreases, the strain reaches the maximum value, which is the ultimate strain of the specimen, and the bearing capacity of the specimen is reduced due to the formation of a macroscopic fracture surface inside. In the fifth stage DE, after the stress is unloaded to a certain value, the total strain of the sandstone specimen will decrease at the tail of the stress-strain curve. The reason for this phenomenon is that although the sandstone specimen is fractured and destabilized, the macroscopic failure pattern of the specimen mainly occurs in the axial splitting failure pattern. During the impact loading process, a part of the energy is converted into elastic energy and stored inside the sandstone specimen; it still has a certain bearing capacity. Therefore, in the stress wave unloading stage, when the loading stress is less than the elastic force stored inside the specimen, the strain stored in the specimen can be quickly released; the deformation of the specimen will rebound slightly, resulting in a decrease in the total strain [27]. This phenomenon is different from the results obtained from the general static load uniaxial compression test.

Figure 12 shows the effect of impact pressure on the dynamic strength of sandstone specimens with different bedding angles. Combined with Table 3 and Figure 12, it can be found that in the dynamic impact test, the impact pressure and bedding angle have a significant impact on the dynamic mechanical properties of the sandstone specimen. Taking Figure 11(a) as an example, the dynamic strength of the specimen with the bedding angle of 0° is 60.93 MPa when the impact pressure is 0.45 MPa. The strength increased to 81.35 MPa and 90.70 MPa when the impact pressure increased to 0.5 MPa and 0.55 MPa, which increased by 33.51% and 48.86%, respectively, showing an obvious strain rate effect [28]. At the same impact pressure, the dynamic compressive strength of the 45° burst-prone sandstone specimen is the lowest.

Comparing the dynamic strength curves of the bedding sandstone under the action of the three impact pressures, it can be found that the dynamic strength of the sandstone specimens with each bedding angle increases with the increase in the impact pressure. The strain rate effect is the most obvious when $\alpha = 0°$. When the impact pressure is 0.45 MPa and 0.5 MPa, the dynamic strength of the specimen is 67.18% and 89.69% of that of the specimen when the impact pressure is 0.55 MPa. The strain rate effect is the least obvious when $\alpha = 45°$; with the increase in impact pressure, the dynamic strength only increased by 8.98% and 11.37%. In conclusion, it can be found that the strain rate effect on the strength of the bedding sandstone specimen is significant, and the strain
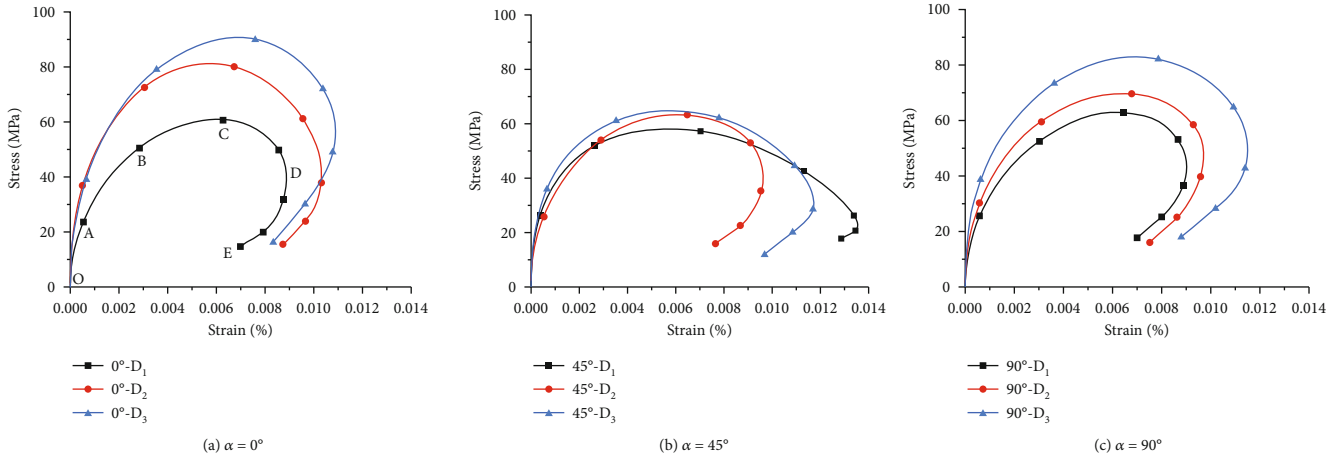
FIGURE 11: Dynamic stress-strain curves of bedding sandstone specimens.

TABLE 3: Mechanical properties of specimens under SHPB tests.

Specimen number	Impact pressure (MPa)	Dynamic strength (MPa)	Strain rate (s^{-1})	Peak strain (%)
$0°\text{-}D_1$	0.45	60.93	34.14	0.00589
$0°\text{-}D_2$	0.50	81.35	47.27	0.00570
$0°\text{-}D_3$	0.55	90.70	52.26	0.00683
$45°\text{-}D_1$	0.45	58.23	33.80	0.00564
$45°\text{-}D_2$	0.50	63.46	36.36	0.00608
$45°\text{-}D_3$	0.55	64.85	39.92	0.00570
$90°\text{-}D_1$	0.45	63.06	36.46	0.00623
$90°\text{-}D_2$	0.50	69.82	40.64	0.00628
$90°\text{-}D_3$	0.55	82.89	50.21	0.00692
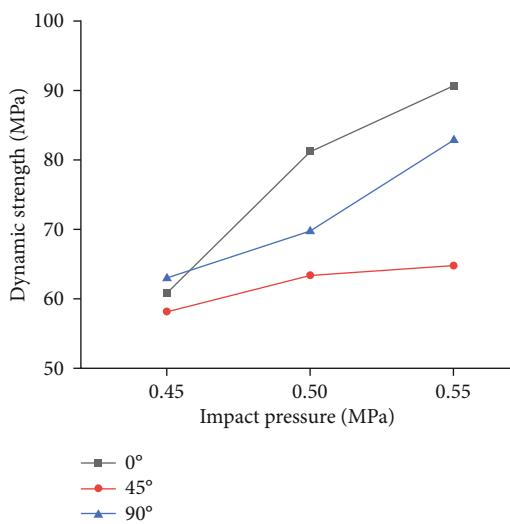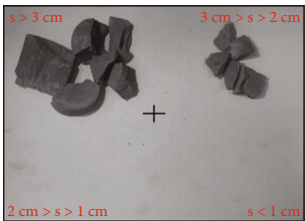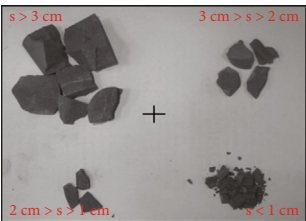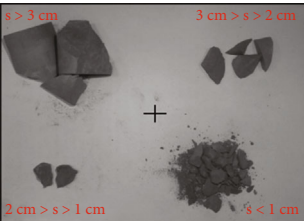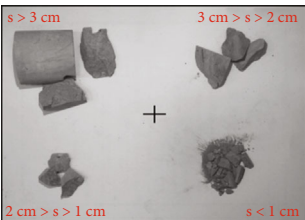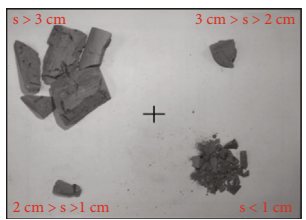
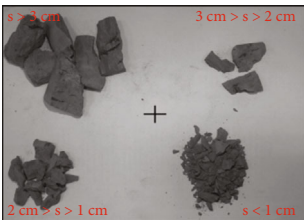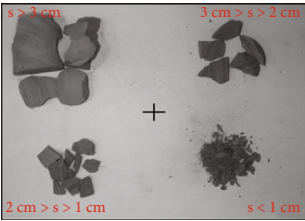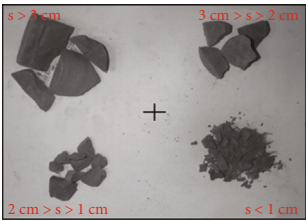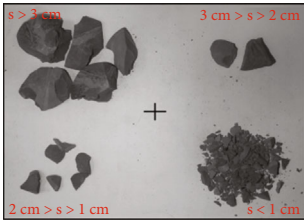FIGURE 12: Dynamic strength of specimens under different impact pressures.

rate effect has different degrees of influence on the specimens with different bedding characteristics.

3.3. Failure Morphological Characteristics of the Bedding Sandstone Specimen under Impact Loads. During the impact loading test, the specimens were damaged to different degrees and produced a large number of fragmented particles. Different impact pressures and bedding angles made the size and shape of the fragments produced by sandstone crushing to be different. Due to the existence of bedding in the sandstone, the fractured sandstone specimens have a typical flaky structure. These fractured products are an important basis for exploring the failure mechanism of bedding sandstone specimens [29]. Therefore, the fragments of the crushed sandstone specimens were collected, and the standard sieves of different sizes (apertures 30 mm, 20 mm, and 10 mm) were used for screening experiments, and the fragmentation range of the crushed products was divided into four grades, respectively: I, $r > 30$ mm; II, 30 mm $\geq r >$ 20 mm; III, 20 mm $\geq r > 10$ mm; and IV, 10 mm $\geq r$; the failure patterns of sandstone specimens under typical impact pressure and bedding angle are shown in Table 4.

It can be seen from Table 4 that under the action of 0.45 MPa impact pressure, the bedding sandstone specimens

TABLE 4: Failure patterns of specimens with different impact pressures and bedding angles.

Bedding angle	Failure patterns		
0°			
45°			
90°			
Impact pressure	0.45 MPa	0.50 MPa	0.55 MPa

have less fine fragments and powders, and the fracture form is mainly reflected in medium and large sandstone fragments, showing a splitting failure pattern. However, under the action of 0.55 MPa impact pressure, the fracture degree of the bedding sandstone specimens is relatively large, and the failure forms are mainly medium and small particle size fragments. With the increase in impact pressure, the crack propagation degree of the bedding sandstone specimen intensifies, and the fracture degree increases gradually, showing a brittle fracture failure form. The particle size of the fragments formed after the failure of the specimen became smaller and the number increased significantly. At the same impact pressure, the fracture degree of the specimen with a bedding angle of 45° is the largest, and the 0° specimen is the smallest. The fragmentation distribution of specimens can well characterize the failure patterns of burst-prone sandstone specimens under different strain rates and indirectly reflect the crushing effect of sandstone specimens under different strain rates [30]. The change of fragmentation distribution of burst-prone sandstone specimens with different bedding angles shows that the failure morphology of the specimens has obvious strain rate effect.

3.4. Summary of the Effect of Bedding Angle on the Dynamic Mechanical Properties of Burst-Prone Sandstone. In this test, three sets of specimens with different bedding angles were prepared for burst-prone sandstone, and the dynamic impact tests were conducted under three different impact pressure conditions using the SHPB test equipment. The anisotropic characteristics of the failure morphological char-

acteristics and dynamic compressive strength of sandstone under dynamic loading conditions due to the influence of bedding angle were studied, and the mechanism of dynamic loading failure of burst-prone sandstones was explored, and the following conclusions were obtained.

(1) The dynamic compressive strength of burst-prone sandstone under three different impact pressure conditions shows a trend of decreasing and then increasing with the change of bedding angle, showing an obvious bedding effect. When $\alpha = 45°$, it is lowest, which is consistent with the strength results obtained from the uniaxial compression test. And the peak stress of the burst-prone specimen under dynamic impact conditions is greater than that of uniaxial compression. Meanwhile, the compressive strength has strain rate effect

(2) For the burst-prone sandstone specimens with the same bedding angle, the particle size gradually decreases as the impact pressure increases, indicating that the fracture degree of the specimen gradually increases. At the same impact pressure, the fracture degree of the specimen with a bedding angle of 45° is the largest, and the 0° specimen is the smallest

4. Discussion

The proneness of rockburst is the result of multiple factors, and the property of surrounding rock is the most basic and

important factor. Due to the fact that the floor of panel 3103 of the Hongqinghe coal mine has significant bedding, the bedding plane is usually used as the boundary of the development and expansion of rock cracks. Through the study of mechanical properties and failure patterns of burst-prone sandstone with different bedding angles under dynamic and static loading conditions, it is revealed that the bedding angle has a weak effect on the static and dynamic mechanical properties of the floor rock mass. The experimental results show that when the bedding angle is 45°, the uniaxial compressive strength and modulus of elasticity of burst-prone sandstone are lower than those of the parallel and vertical bedding, which is prone to failure. According to the dynamic impact test and the analysis of fragmentation distribution, the dynamic compressive strength of the 45° burst-prone sandstone specimen is significantly lower than that of other bedding angle specimens, and its fracture degree is the most severe, so it can be speculated that its resistance to dynamic load is the worst. Based on the results obtained in the uniaxial compression test and dynamic impact test, the proneness for rockburst to occur can be further clarified.

Field observations indicate that cracks will preferentially follow these bedding weak planes, leading to tensile and shear failures. At the same time, excessive tensile crack will be generated on the weak plane. All of these exacerbate the development of the bedding planes, leading to significant deformation and severe rockburst disasters [31]. Therefore, it is reasonable to predict that the in situ rock mass of panel 3103 also has a similar failure mechanism as revealed in the experiments.

In the process of underground mining, the surrounding rock of the roadway continuously accumulates elastic energy under the action of in situ stress. When the in situ stress continues to increase, a large amount of elastic energy accumulates in the surrounding rock. After strong dynamic disturbance, when the superposition of the static load and dynamic load in the coal and rock mass is greater than the minimum load that induces the impact failure of the coal and rock mass, the accumulated elastic energy will be released suddenly, causing dynamic disasters such as roof fall and rockburst.

The presented laboratory tests revealed that the bedding angle in burst-prone sandstone is an important factor to assess rockburst proneness [32]. In the production process of underground rock mass engineering, the bedding sandstone is susceptible to various dynamic disturbances, so the experimental and theoretical research on bedding sandstone under dynamic load has important reference and guiding significance for production and development [33–35]. In this paper, a preliminary study on the bedding effect of burst-prone sandstone under uniaxial static and dynamic loading is carried out, and for further study, more tests on burst-prone sandstone with other types of bedding angle under coupled static and dynamic loads should be carried out to analyze its influence on rockburst occurrence.

5. Conclusions

In this paper, the mechanical properties and failure characteristics of sandstone specimens with different bedding angles under static and dynamic loads were investigated by the MTS816 rock mechanics testing system and the SHPB experimental system, respectively. Based on the experimental results, the conclusions are summarized as follows:

(1) Bedding angle has an important effect on the uniaxial compressive strength and failure pattern of sandstone. The order of uniaxial compressive strength of sandstone specimen with different bedding angles is that $0° > 90° > 45°$. The sandstone specimen at $\alpha = 0°$ mainly shows splitting damage and local compression expansion; the sandstone specimen at $\alpha = 45°$ mostly shows slip shear damage along the bedding plane; the sandstone specimen at $\alpha = 90°$ shows a conical failure pattern

(2) By conducting SHPB tests under different impact pressure conditions, it is found that the dynamic strength of the specimens is positively correlated with the impact pressure, showing an obvious strain rate effect. The dynamic compressive strength of the 45° burst-prone sandstone specimen is the lowest

(3) In the dynamic mechanical property test, the broken pieces of the crushed sandstone specimens are collected. With the increase in impact pressure, the degree of brokenness of the bedding sandstone specimens gradually increases, and the particle size of the broken pieces become smaller, and the number increases significantly. At the same impact pressure, the fracture degree of the specimen with a bedding angle of 45° is the largest, showing a brittle fracture failure form, and the 0° specimen is the smallest. The effect of dynamic load on the degree of specimen fragmentation is greater than that of static load

Data Availability

Data used to support the results of this study can be found in this manuscript text.

Conflicts of Interest

The authors declare that they have no known competing financial interests or personal relationships that could have appeared to influence the work reported in this paper.

Acknowledgments

References

[1] B. H. G. Brady and E. T. Brown, *Rock Mechanics for Underground Mining*, Springer, Netherlands, 2006.

[2] X. Chang, Y. F. Shan, Z. H. Zhang, C. A. Tang, and Z. L. Ru, "Behavior of propagating fracture at bedding interface in layered rocks," *Engineering Geology*, vol. 197, pp. 33–41, 2015.

[3] P. F. Yin and S. Q. Yang, "Discrete element modeling of strength and failure behavior of transversely isotropic rock under uniaxial compression," *Journal of the Geological Society of India*, vol. 93, no. 2, pp. 235–246, 2019.

[4] K. Bo-Hyun, W. Gabriel, M. K. Larson, and B. Steve, "Investigation of the anisotropic confinement-dependent brittleness of a Utah coal," *International Journal of Rock Mechanics and Mining Sciences*, vol. 8, no. 2, pp. 274–290, 2021.

[5] Y. M. Tien and M. C. Kuo, "A failure criterion for transversely isotropic rocks," *International Journals of Rock Mechanic and Mining Science*, vol. 38, no. 3, pp. 399–412, 2001.

[6] C. C. Wang, J. T. Li, H. Lin, J. Liao, P. Wang, and S. Wang, "Anisotropic mechanical characteristics of slate in uniaxial compression," *Journal of Central South University (Science and Technology)*, vol. 47, no. 11, pp. 3759–3764, 2016.

[7] A. Tavallali and A. Vervoort, "Failure of layered sandstone under Brazilian test conditions: effect of micro-scale parameters on macro-scale behaviour," *Rock Mechanics and Rock Engineering*, vol. 43, no. 5, pp. 641–653, 2010.

[8] S. Q. Yang, P. F. Yin, B. Li, and D. S. Yang, "Behavior of transversely isotropic shale observed in triaxial tests and Brazilian disc tests," *International Journal of Rock Mechanics and Mining Sciences*, vol. 133, article ???, 2020.

[9] Y. Y. Zhou, X. T. Feng, D. P. Xu, and Q. X. Fan, "An enhanced equivalent continuum model for layered rock mass incorporating bedding structure and stress dependence," *International Journal of Rock Mechanics and Mining Sciences*, vol. 97, pp. 75–98, 2017.

[10] D. Y. Li, Z. Y. Han, X. L. Sun, T. Zhou, and X. B. Li, "Dynamic mechanical properties and fracturing behavior of marble specimens containing single and double flaws in SHPB tests," *Rock Mechanics and Rock Engineering*, vol. 52, pp. 1623–1643, 2018.

[11] X. M. Zhang, X. F. Ou, F. Q. Gong, and J. S. Yang, "Effects of bedding on the dynamic compressive properties of low anisotropy slate," *Rock Mechanics and Rock Engineering*, vol. 52, no. 4, pp. 981–990, 2019.

[12] J. D. Qiu, D. Y. Li, and X. B. Li, "Dynamic failure of a phyllite with a low degree of metamorphism under impact Brazilian test," *International Journal of Rock Mechanics and Mining Sciences*, vol. 94, pp. 10–17, 2017.

[13] X. H. Liu, F. Dai, R. Zhang, and J. F. Liu, "Static and dynamic uniaxial compression tests on coal rock considering the bedding directivity," *Environmental Earth Sciences*, vol. 73, no. 10, pp. 5933–5949, 2015.

[14] H. K. Gao, Q. Wang, B. Jiang, P. Zhang, Z. H. Jiang, and Y. Wang, "Relationship between rock uniaxial compressive strength and digital core drilling parameters and its forecast method," *International Journal of Coal Science and Technology*, vol. 8, no. 4, pp. 605–613, 2021.

[15] C. E. Fairhurst and J. A. Hudson, "Draft ISRM suggested method for the complete stress-strain curve for intact rock in uniaxial compression," *International Journal of Rock Mechanics and Mining Sciences*, vol. 36, no. 3, pp. 279–289, 1999.

[16] B. Liu, Y. X. Zhao, C. Zhang, J. L. Zhou, Y. T. Li, and Z. Sun, "Characteristic strength and acoustic emission properties of weakly cemented sandstone at different depths under uniaxial compression," *International Journal of Coal Science and Technology*, vol. 8, no. 6, pp. 1351–1370, 2021.

[17] H. Wang, T. H. Yang, and Y. J. Zuo, "Experimental study on acoustic emission of weakly cemented sandstone considering bedding angle," *Shock and Vibration*, vol. 2018, Article ID 6086583, 12 pages, 2018.

[18] P. L. P. Wasantha, P. G. Ranjith, and S. S. Shao, "Energy monitoring and analysis during deformation of bedded-sandstone: use of acoustic emission," *Ultrasonics*, vol. 54, no. 1, pp. 217–226, 2014.

[19] Y. Y. Zhou, X. T. Feng, D. P. Xu, and Q. X. Fan, "Experimental investigation of the mechanical behavior of bedded rocks and its implication for high sidewall caverns," *Rock Mechanics and Rock Engineering*, vol. 49, no. 9, pp. 3643–3669, 2016.

[20] J. Yu, W. Yao, K. Duan, X. Y. Liu, and Y. L. Zhu, "Experimental study and discrete element method modeling of compression and permeability behaviors of weakly anisotropic sandstones," *International Journal of Rock Mechanics and Mining Sciences*, vol. 134, p. 104437, 2020.

[21] Q. B. Zhang and J. Zhao, "A review of dynamic experimental techniques and mechanical behaviour of rock materials," *Rock Mechanics and Rock Engineering*, vol. 47, no. 4, pp. 1411–1478, 2013.

[22] H. Kolsky, "Stress waves in solids," *Journal of Sound and Vibration*, vol. 1, no. 1, pp. 88–110, 1964.

[23] D. Y. Li, M. Liu, Z. Y. Han, and Z. L. Zhou, "Dynamic compressive mechanical properties of bedding sandstone with pre-existing hole," *Journal of China Coal Society*, vol. 44, no. 5, pp. 1349–1358, 2019.

[24] X. B. Li, T. Zhou, and D. Y. Li, "Dynamic strength and fracturing behavior of single-flawed prismatic marble specimens under impact loading with a split-Hopkinson pressure bar," *Rock Mechanics and Rock Engineering*, vol. 50, no. 1, pp. 29–44, 2017.

[25] D. Y. Li, Z. Y. Han, Q. Q. Zhu, Y. Zhang, and P. G. Ranjith, "Stress wave propagation and dynamic behavior of red sandstone with single bonded planar joint at various angles," *International Journal of Rock Mechanics and Mining Sciences*, vol. 117, pp. 162–170, 2019.

[26] Y. X. Zhao, G. F. Zhao, Y. D. Jiang, D. Elsworth, and Y. Q. Huang, "Effects of bedding on the dynamic indirect tensile strength of coal: laboratory experiments and numerical simulation," *International Journal of Coal Geology*, vol. 132, pp. 81–93, 2014.

[27] X. B. Li, F. Q. Gong, J. Zhao, K. Gao, and T. Yin, "Test study of impact failure of rock subjected to one-dimensional coupled static and dynamic loads," *Chinese Journal of Rock Mechanics and Engineering*, vol. 29, no. 2, pp. 251–260, 2010.

[28] F. Q. Gong, H. Ye, and Y. Luo, "The effect of high loading rate on the behaviour and mechanical properties of coal-rock combined body," *Shock and Vibration*, vol. 2018, Article ID 4374530, 9 pages, 2018.

[29] Y. Deng, M. Chen, Y. Jin, and D. W. Zou, "Theoretical analysis and experimental research on the energy dissipation of rock crushing based on fractal theory," *Journal of Natural Gas Science and Engineering*, vol. 33, pp. 231–239, 2016.

[30] X. F. Li, H. B. Li, Q. B. Zhang, J. L. Jiang, and J. Zhao, "Dynamic fragmentation of rock material: characteristic size, fragment distribution and pulverization law," *Engineering Fracture Mechanics*, vol. 199, pp. 739–759, 2018.

[31] B. Chen, "Stress-induced trend: the clustering feature of coal mine disasters and earthquakes in China," *International*

Journal of Coal Science and Technology, vol. 7, no. 4, pp. 676–692, 2020.

[32] M. C. He, W. Nie, Z. Y. Zhao, and W. Guo, "Experimental investigation of bedding plane orientation on the rockburst behavior of sandstone," *Rock Mechanics and Rock Engineering*, vol. 45, no. 3, pp. 311–326, 2012.

[33] S. Heng, Y. T. Guo, C. H. Yang, J. J. K. Daemen, and Z. Li, "Experimental and theoretical study of the anisotropic properties of shale," *International Journal of Rock Mechanics and Mining Sciences*, vol. 74, pp. 58–68, 2015.

[34] S. F. Wang, L. C. Sun, X. B. Li et al., "Experimental investigation of cuttability improvement for hard rock fragmentation using conical cutter," *International Journal of Geomechanics*, vol. 21, no. 2, article 06020039, 2021.

[35] S. F. Wang, Y. Tang, X. B. Li, and K. Du, "Analyses and predictions of rock cuttabilities under different confining stresses and rock properties based on rock indentation tests by conical pick," *Transactions of Nonferrous Metals Society of China*, vol. 31, no. 6, pp. 1766–1783, 2021.